

Partial observations, coarse graining and equivariance in Koopman operator theory for large-scale dynamical systems

Sebastian Peitz,¹ Hans Harder,¹ Feliks Nüske,²
Friedrich Philipp,³ Manuel Schaller,³ Karl Worthmann³

¹ Department of Computer Science, Paderborn University, Paderborn, Germany

² Max Planck Institute for Dynamics of Complex Technical Systems, Magdeburg, Germany

³ Optimization-based Control Group, TU Ilmenau, Ilmenau, Germany

{sebastian.peitz, hans.harder}@upb.de, nueske@mpi-magdeburg.mpg.de,
{friedrich.philipp, manuel.schaller, karl.worthmann}@tu-ilmenau.de

Abstract

The Koopman operator has become an essential tool for data-driven analysis, prediction and control of complex systems, the main reason being the enormous potential of identifying linear function space representations of nonlinear dynamics from measurements. Until now, the situation where for large-scale systems, we (i) only have access to partial observations (i.e., measurements, as is very common for experimental data) or (ii) deliberately perform coarse graining (for efficiency reasons) has not been treated to its full extent. In this paper, we address the pitfall associated with this situation, that the classical EDMD algorithm does not automatically provide a Koopman operator approximation for the underlying system if we do not carefully select the number of observables. Moreover, we show that symmetries in the system dynamics can be carried over to the Koopman operator, which allows us to massively increase the model efficiency. We also briefly draw a connection to domain decomposition techniques for partial differential equations and present numerical evidence using the Kuramoto–Sivashinsky equation.

Introduction

Many phenomena in nature can be described by *partial differential equations (PDEs)*, where the system state depends both on space and time. Popular examples are fluid dynamics or electromagnetics. Studying such systems poses many challenges, including sophisticated numerical discretization schemes (using, e.g., finite elements), a very high dimension of the resulting discretized nonlinear systems, and the challenge that in real experiments, the entire system state is accessible in few cases only. Finally, we only have very crude models (if at all) for some systems, e.g., from biology.

Due to these reasons, there has been an increasing interest in the scientific community to develop and improve methods to infer and predict dynamical systems from data. Popular examples are the *Sparse Identification of Nonlinear Dynamics* (Brunton, Proctor, and Kutz 2016), statistical approaches such as the *Mori-Zwanzig* framework (Chorin, Hald, and Kupferman 2000), or techniques based on deep learning (Vlachas et al. 2018), also using physical knowledge (Raissi, Perdikaris, and Karniadakis 2019). Another approach that has been particularly successful in the past decade is the *Koopman operator* framework (Koopman 1931; Rowley

et al. 2009; Mezić 2013). The driving force behind this renaissance is twofold: (1) The Koopman operator yields a linear representation of nonlinear dynamical systems, thus giving us access to powerful techniques from linear systems theory, and (2) the advances in numerical approximation (here in the form of the *Extended Dynamic Mode Decomposition (EDMD)* (Williams, Kevrekidis, and Rowley 2015; Klus, Koltai, and Schütte 2016; Klus et al. 2020)) now allow us to identify the Koopman operator from measurements using simple linear regression. As a consequence, the Koopman operator has been studied extensively for data-driven analysis (Brunton et al. 2022), coarse graining (Boninsegna, Nüske, and Clementi 2018; Klus et al. 2020; Niemann, Klus, and Schütte 2021; Nüske et al. 2021) and control (Proctor, Brunton, and Kutz 2015; Korda and Mezić 2018a; Peitz and Klus 2019; Peitz, Otto, and Rowley 2020; Schaller et al. 2023) of a very large number of applications from neuroscience over social systems and robotics to fluid dynamics. Besides, a formal treatment of Koopman operator methods for PDEs was addressed in Nakao and Mezić (2020); Mauroy (2021), and recent results on finite-data error bounds can be found in Zhang and Zuazua (2023); Nüske et al. (2023); Philipp et al. (2023); Bevanda et al. (2023).

Contributions:

- Even though the Koopman operator allows for arbitrary observations, there are severe pitfalls when we do not know or cannot efficiently discretize the system’s state space. Many articles simply use the *full state observable*, which greatly simplifies the situation. Here, we address this issue in detail and derive rigorous conditions on partial observations that rely on fundamental embedding theorems.
- There is only little literature on Koopman operators for systems with symmetries; see, e.g., Salova et al. (2019) for ordinary differential equations, or Weissenbacher et al. (2022), where the matrix approximation of the Koopman operator was used to heuristically identify symmetries in Markov Decision Processes. Here, we provide a systematic treatment of symmetries in PDEs, which will allow us to significantly increase the numerical performance of the Koopman operator approximation. Furthermore, our approach allows us to transfer a learned Koopman approximation from one domain to another without retraining.
- We draw a connection between our equivariant Koop-

man formulation to well-established domain decomposition methods for PDEs.

Koopman operator for PDEs

We start by introducing the Koopman operator for partial differential equations, although everything that follows applies equally to ordinary differential equations (ODEs). Consider the general dynamical system

$$\frac{\partial y}{\partial t} = \mathcal{N}(y), \quad y(\cdot, 0) = y_0. \quad (1)$$

Here, $y(x, t)$ is the space- and time-dependent system state, $t \in \mathbb{R}_{\geq 0}$ is the time and $x \in \Omega$ the spatial coordinate (for now one-dimensional). Moreover, $y(\cdot, t) \in L^2(\Omega)$ and $\mathcal{N} : D(\mathcal{N}) \rightarrow L^2(\Omega)$ (with $D(\mathcal{N}) \subset L^2(\Omega)$ being the domain of \mathcal{N}) is a nonlinear partial differential operator describing the dynamics of the system. We assume periodic boundary conditions (BCs). The system's flow map $\Phi^\tau : L^2(\Omega) \rightarrow L^2(\Omega)$ is defined by

$$y(\cdot, t + \tau) = \Phi^\tau(y(\cdot, t)).$$

Furthermore, we assume that the system possesses an invariant compact set $\mathcal{A} \subset D(\mathcal{N})$, i.e., $\Phi^\tau(\mathcal{A}) = \mathcal{A}$, which has dimension $\dim(\mathcal{A}) = d$ (often, the *box counting dimension* is used in this context (Ziessler, Dellnitz, and Gerlach 2019)). Usually, \mathcal{A} is the system's *attractor* or an *invariant manifold*, and it is well known that many PDEs possess an attractor with $d < \infty$.

Example 1. *The well-known Kuramoto–Sivashinsky equation that we will study in this paper is, in dimensionless form,*

$$\frac{\partial y}{\partial t} + 4 \frac{\partial^4 y}{\partial x^4} + \mu \left[\frac{\partial^2 y}{\partial x^2} + y \frac{\partial y}{\partial x} \right] = 0 \quad (2)$$

on the domain $\Omega = [0, L] = [0, 2\pi]$ with $\mu \in (0, \infty)$. Depending on μ , the system exhibits rich dynamics, from bimodal fixed points to traveling waves to fully chaotic behavior (Hyman, Nicolaenko, and Zaleski 1986). Moreover, one can bound the dimension of the attractor \mathcal{A} in terms of the domain size L via $d \leq L^{2.46}$ when not considering the non-dimensionalized version as we do in (2), see Ziessler, Dellnitz, and Gerlach (2019) for more details.

The *semigroup of Koopman operators* associated with (1) is defined on a space of observable functionals, see (Mauroy 2021).

Definition 2 (Koopman semigroup and generator). *Consider the space $C(\mathcal{A})$ of continuous real-valued functionals $f : \mathcal{A} \rightarrow \mathbb{R}$, endowed with the supremum norm $\|f\| = \sup_{y \in \mathcal{A}} |f(y)|$. The semigroup of Koopman operators $(\mathcal{K}^\tau)_{\tau \geq 0}$ associated with the semiflow $(\Phi^\tau)_{\tau \geq 0}$ is defined by*

$$\mathcal{K}^\tau f = f \circ \Phi^\tau, \quad f \in C(\mathcal{A}). \quad (3)$$

The *Lie generator of the semigroup* is the linear operator $\mathcal{K} : D(\mathcal{K}) \rightarrow C(\mathcal{A})$ that satisfies

$$\mathcal{K}f = \lim_{\tau \rightarrow 0} \frac{\mathcal{K}^\tau f - f}{\tau}. \quad (4)$$

Remark 3. *An extension to vector-valued observable functions $f : \mathcal{A} \rightarrow \mathbb{R}^q$ in $C(\mathcal{A})^q$ can be realized in a straightforward manner, see, e.g., (Budišić, Mohr, and Mezić 2012).*

In the case of a Koopman semigroup associated with a semiflow generated by the PDE (1), it follows from the chain rule that the generator is given by

$$(\mathcal{K}f)(y) = D_{\mathcal{N}(y)}f(y), \quad (5)$$

which can be interpreted as the Lie derivative associated with the infinite-dimensional vector field \mathcal{N} , where $D_{\mathcal{N}(y)}f(y)$ denotes the (linear) Gâteaux derivative of f at y in the direction $\mathcal{N}(y)$. Note that this is closely related to the generator PDE that we find for ODEs (Klus et al. 2020). An alternative derivation using the functional derivative can be found in Nakao and Mezić (2020).

Even though the Koopman operator formalism has been known for a very long time, it has received a massive increase in attention in the past decade, mostly due to the advances in its numerical approximation via EDMD. Based on the observation that Eqs. (3) and (4) are linear, we can try to compute finite-dimensional approximations $K^\tau \in \mathbb{R}^{\ell \times \ell}$ and $K \in \mathbb{R}^{\ell \times \ell}$ to \mathcal{K}^τ and \mathcal{K} , respectively. We achieve this via Galerkin projection by introducing a finite dictionary $\{\psi_j\}_{j=1}^\ell$ of functions $\psi_j \in C(\mathcal{A})^q$, and coefficients $a \in \mathbb{R}^\ell$:

$$f(y(\cdot, t)) \approx \sum_{j=1}^{\ell} a_j \psi_j(y(\cdot, t)) = a^\top \Psi(y(\cdot, t)). \quad (6)$$

Using observed time series data $[\Psi(y_0), \Psi(y_1), \dots, \Psi(y_m)]$, where $y_i = y(\cdot, i\tau)$ and $\Psi = [\psi_1^\top, \dots, \psi_\ell^\top]^\top : \mathcal{A} \rightarrow \mathbb{R}^{\ell q}$, we can now simply use linear regression to find the best fit matrix K^τ :

$$\min_{K^\tau \in \mathbb{R}^{\ell q \times \ell q}} \sum_{i=0}^{m-1} \|\Psi(y_{i+1}) - K^\tau \Psi(y_i)\|_2^2. \quad (7)$$

A very similar regression problem can be formulated to approximate the generator \mathcal{K} via K (Klus et al. 2020). In both cases, it can be shown that this matrix converges to the Galerkin projection of \mathcal{K}^τ in the infinite data limit $m \rightarrow \infty$ (Williams, Kevrekidis, and Rowley 2015; Klus, Koltai, and Schütte 2016), and to the true Koopman operator when additionally $\ell \rightarrow \infty$ (Korda and Mezić 2018b). Moreover, finite-data error bounds can be found in Zhang and Zuazua (2023); Nüske et al. (2023); Philipp et al. (2023); Bevanda et al. (2023), using either i.i.d. or ergodic sampling.

Partial measurements, coarse graining & unknown state spaces

A large part of the existing literature focuses on small-scale systems or the situation where f is the identity mapping, i.e., the *full state observable*. Alternatively, it is at least assumed that the state space (here: $L^2(\Omega)$) is known and that the observable f can be numerically approximated in an efficient manner. (An exception is Otto, Peitz, and Rowley (2022), where a Kalman filter was used to infer the state of an unknown system from measurements.) However, this

viewpoint has severe limitations. If, for instance, we consider PDEs, the state space may be challenging to approximate numerically. Moreover, if the data stems from real experiments, the domain may be unknown altogether. The same challenges occur in large-scale systems of ODEs such as molecular dynamics, agent-based systems or dynamics on graphs (e.g., electric grids, where the entire graph is not necessarily known). In this situation, a coarse graining to meaningful macro observables (Zhang, Hartmann, and Schütte 2016; Boninsegna, Nüske, and Clementi 2018; Niemann, Klus, and Schütte 2021; Nüske et al. 2021) is highly desirable, at the cost of loosing knowledge of the underlying dynamical equations.

A common pitfall of partial measurements

In the following, we will precisely consider the above-described situation where we do not necessarily know f or the state space, not to mention the attractor \mathcal{A} . Formally, there still exists an observable $f : \mathcal{A} \rightarrow \mathbb{R}^q$, according to which we collect our measurements $z_i = f(y_i)$. However, as we are ignorant of f or the domain \mathcal{A} , we appear to be at an impasse: we cannot define a dictionary $\{\psi_j\}_{j=1}^\ell$ in $C(\mathcal{A})^q$, which is the key step in EDMD, cf. Eqs. (6)–(7).

A practical means to overcome this impasse is to collect measurements $z = [z_0, z_1, \dots, z_m] \in \mathbb{R}^{q \times (m+1)}$, where $z_i = f(y_i)$, and try to approximate the Koopman operator directly from the data. If the measurement is low-dimensional (i.e., q is small) people often simply *lift* the data z using a dictionary such as delay coordinates or polynomials with maximal degree s , i.e.,

$$\Psi(z) = [1 \quad z_1 \quad \dots \quad z_q \quad z_1^2 \quad z_1 z_2 \quad \dots \quad z_q^s]^\top. \quad (8)$$

Examples of this approach are, e.g., lift and drag measurements of a fluid flow (Peitz and Klus 2019), coarse-grained coordinates of large molecules (Nüske et al. 2021) or delay coordinates of highway traffic data (Avila and Mezić 2020). However, this approach provides a major pitfall when it comes to learning anything about the dynamics of the original system. Conceptually, we treat our measurements in such a way that we now use the full state observable on a different, implicitly defined dynamical system $\varphi^\tau : \mathbb{R}^q \rightarrow \mathbb{R}^q$ that describes the dynamics of the observed quantity z on the artificial state space \mathbb{R}^q :

$$z_{i+1} = \varphi^\tau(z_i). \quad (9)$$

Following Dellnitz, Hessel-von Molo, and Ziessler (2016); Ziessler, Dellnitz, and Gerlach (2019), we will call (9) the *Core Dynamical System (CDS)*.

Assuming that the CDS exists and is uniquely defined, we can now define a new observable $h \in \mathcal{H} = C(f(\mathcal{A}))^q$, $h : \mathbb{R}^q \rightarrow \mathbb{R}^q$ whose domain is now the state space of the CDS. In this setting, we can simply apply EDMD in its standard form (Eqs. (6)–(7) in combination with a dictionary as in (8)), to identify the Koopman operator associated with the CDS and the observable function h .¹ This concept is illus-

¹For convenience, we will use the full state observable $h = \text{id}$ here, but our equivalence result in Theorem 6 also covers the more general setting for arbitrary h .

trated in Fig. 1, where $z = h(z) = h(f(y))$, and $\{\psi_j\}_{j=1}^\ell$ spans a subspace of \mathcal{H} instead of $C(\mathcal{A})$.

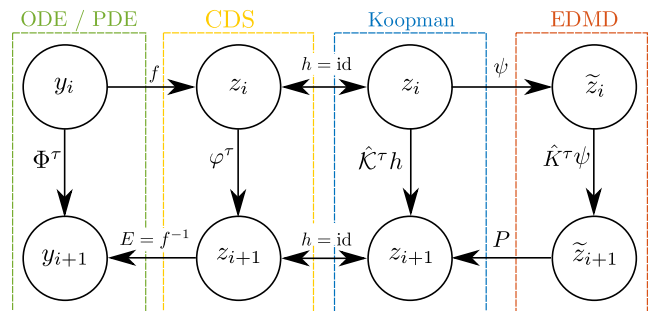


Figure 1: The extended Koopman operator concept for partially observed or unknown states. Instead of directly learning the Koopman operator for the observable $f : \mathcal{Y} \rightarrow \mathbb{R}^q$, we introduce the core dynamical system φ^τ as an intermediate model that – given a sufficiently large embedding dimension q – has a one-to-one correspondence to Φ^τ on the attractor. The Koopman operator is then defined in the standard ODE setting using a new observable function $h \in \mathcal{H}$, $h : \mathbb{R}^q \rightarrow \mathbb{R}^q$. For simplicity, we choose $h = \text{id}$ here.

Relation between the Core Dynamical System and the underlying PDE

What remains to be shown is the correspondence between the original dynamical system Φ^τ and the corresponding CDS φ^τ . To this end, we closely follow the approach in Ziessler, Dellnitz, and Gerlach (2019) and make use of well-known embedding theorems such as Whitney (1936), Takens (1981), or Robinson (2005). For a detailed discussion on the more intricate implications of the following theorem – as well as the definitions of the terms *box counting dimension*, *thickness exponent* (which is usually $\sigma = 0$) and *prevalence* – we refer the reader to Ziessler, Dellnitz, and Gerlach (2019).

Theorem 4 (Robinson (2005); Ziessler, Dellnitz, and Gerlach (2019)). *Let $\mathcal{A} \subset \mathcal{Y}$ be a compact, invariant set, with upper box counting dimension $\dim(\mathcal{A}) = d$, and thickness exponent σ . Choose an integer $q > 2(1 + \sigma)d$, and suppose further that the set \mathcal{A}_p of p -periodic points of Φ^τ satisfies $\dim(\mathcal{A}_p) < p/(2 + 2\sigma)$ for $p = 1, \dots, q$. Then for almost every (in the sense of prevalence) Lipschitz map $g : \mathcal{Y} \rightarrow \mathbb{R}$ the delay observation map $f := D_q[g, \Phi^\tau] : \mathcal{Y} \rightarrow \mathbb{R}^q$ defined by*

$$y \mapsto [g(y) \quad g(\Phi^\tau(y)) \quad \dots \quad g(\Phi^{(q-1)\tau}(y))]^\top$$

is one-to-one on \mathcal{A} . The same holds for a set of q distinct observables $g_1, \dots, g_q : \mathcal{Y} \rightarrow \mathbb{R}$, i.e.,

$$f = [g_1(y) \quad \dots \quad g_q(y)]^\top.$$

Remark 5. *The central message of the above theorem is that we can draw a close connection between the observable f in the Koopman setting (Definition 2 and Remark 3) and the observation map g in the embedding framework. The key*

statement for our purposes is that if the system dynamics of Φ^τ is restricted to a compact set \mathcal{A} with a finite dimension d , then we need to have at least $q > 2d$ distinct measurements g – which jointly form the Koopman observable f – to obtain a one-to-one correspondence between Φ^τ and φ^τ :

$$\Phi^\tau = E \circ \varphi^\tau \circ D_q[g, \Phi^\tau] = E \circ \varphi^\tau \circ f,$$

where E is the inverse of f . This way, the CDS becomes:

$$\varphi^\tau = f \circ \Phi^\tau \circ f^{-1}. \quad (10)$$

As a consequence, we can relate the Koopman operator for φ^τ to the Koopman operator for Φ^τ .

Theorem 6. *Let the assumptions of Theorem 4 hold and define the Koopman operator \mathcal{K}^τ for the PDE (1) in its standard form as in (3). Furthermore, define the Koopman operator for the CDS φ^τ with observable $h : \mathbb{R}^q \rightarrow \mathbb{R}^p$ as follows:*

$$\hat{\mathcal{K}}^\tau h = h \circ \varphi^\tau, \quad h \in \mathcal{H}.$$

Then $h \circ \mathcal{K}^\tau f = \hat{\mathcal{K}}^\tau h \circ f$. Moreover, we find that \mathcal{K}^τ and $\hat{\mathcal{K}}^\tau$ share the same spectrum, and the eigenfunctions are related via f .

Proof. The proof immediately follows from the one-to-one correspondence established in Theorem 4, which means that for every $z \in f(\mathcal{A})$ we find exactly one $y \in \mathcal{A}$ such that $f(y) = z$. Choose an arbitrary $y_0 \in \mathcal{A}$ with $y_1 = \Phi^\tau(y_0) \in \mathcal{A}$ (we have $y_1 \in \mathcal{A}$ due to the invariance of \mathcal{A}). Then

$$\begin{aligned} h((\mathcal{K}^\tau f)(y_0)) &= h(f(\Phi^\tau(y_0))) = h(f(y_1)) = h(z_1) \\ &= h(\varphi^\tau(z_0)) = (\hat{\mathcal{K}}^\tau h)(z_0) = (\hat{\mathcal{K}}^\tau h)(f(y_0)) \\ &= (\hat{\mathcal{K}}^\tau h \circ f)(y_0). \end{aligned}$$

For the spectrum, consider an eigenfunction $\hat{\xi}$ with associated eigenvalue $\hat{\lambda}$ such that

$$\hat{\mathcal{K}}^\tau \hat{\xi} = \hat{\lambda} \hat{\xi}.$$

Then, using Eq. (10) and introducing $\xi = \hat{\xi} \circ f$, we find

$$\begin{aligned} \hat{\xi} \circ \varphi^\tau &= \hat{\xi} \circ f \circ \Phi^\tau \circ f^{-1} = \hat{\lambda} \hat{\xi} \\ \Leftrightarrow \hat{\xi} \circ f \circ \Phi^\tau &= \hat{\lambda} \hat{\xi} \circ f \\ \Leftrightarrow \xi \circ \Phi^\tau &= \hat{\lambda} \xi. \end{aligned}$$

□

Remark 7. For $h = \text{id}$, we find $\mathcal{K}^\tau f = \hat{\mathcal{K}}^\tau h \circ f$.

Equivariant Koopman operators for equivariant PDEs and convolution observables

We now want to make use of the above-mentioned partial observations in order to approximate local, spatially confined Koopman operators for partial differential equations (PDEs) that possess symmetries. That means, instead of measuring the entire state, we will only utilize point measurements from a small subregion of the spatial domain. We are going to realize this by means of a convolution observable, which as a special case yields point measurements, but covers many other settings as well.

In order to discuss the basic symmetry concepts, let us forget about the time dependence of y for a moment and instead denote the state at a fixed time t by $y_t(x) = y(x, t)$ for $x \in \Omega$. For a more detailed introduction, see (Bronstein et al. 2021). A *group* is a set G along with an associative composition operation $\circ : G \times G \rightarrow G$ that contains an identity and inverses. A *group action* of G on a set Ω is then defined as a mapping $(g, x) \rightarrow g[x]$ associating a group element $g \in G$ and a point $x \in \Omega$ with some other point in Ω in a way that is compatible with the group operations, i.e., $g[(h[x])] = (gh)[x]$ for all $g, h \in G$ and $x \in \Omega$.

Example 8. *The Euclidean group $E(2)$ in the plane is the group of transformations of \mathbb{R}^2 that preserves Euclidean distances, consists of translations, rotations, and reflections. The same group can also act on the space of functions on the plane, that is, if we have a group G acting on Ω , we automatically obtain an action of G on the space $\mathcal{Y}(\Omega)$: $g[y_t](x) = y_t(g^{-1}[x])$. Due to the inverse on g , this is indeed a valid group action, in that we have $(g[(h[y_t]]))(x) = ((gh)[y_t])(x)$.*

For the subset of linear group actions, we can define group representations $T_g : \Omega \rightarrow \Omega$. If T_g satisfies $y_t(x) = y_t(T_g x)$ for all $g \in G$ and $x \in \Omega$, then we say that y_t is *invariant* or *symmetric* to T_g and that $\{T_g\}_{g \in G}$ is a set of symmetries of y_t . A related notion is *equivariance*. Given a transformation map $T_g : \Omega \rightarrow \Omega$ and some $y_t \in \mathcal{Y}$, we say that y_t is *equivariant* to the transformation if there exists a second transformation operator $T'_g : \mathcal{Y} \rightarrow \mathcal{Y}$ in the output space of y_t such that $T'_g y_t(x) = y_t(T_g x)$ for all $g \in G$, $y_t \in \mathcal{Y}$. The operators T_g and T'_g can be seen as describing the same transformation, but in different spaces. Invariance is a special case of equivariance, if we set T'_g to the identity for all g .

Let us now define a particular observable, namely the *Convolution operator*. Generally, a convolution is the composition of two functions which produces another function in a new coordinate. Usually, a function of interest (e.g., our system state y) is composed with a kernel θ :

$$(y_t \star \theta)(s) = \int_{\Omega} y_t(x) \theta(s - x) dx.$$

In many situations, θ is a Gaussian kernel that somewhat “localizes” y_t around the center s (even though not in a strict sense, of course). Now, fixing s , we can define the observable function

$$f_s(y_t) = z_t(s) = (y_t \star \theta)(s). \quad (11)$$

Remark 9. *Eq. (11) is very general, as it includes point observables (using a Dirac-Delta kernel) as well as integrals over parts of the domain. An extension to more complex expressions (i.e., nonlinear functions of the full state y) can be realized in a straightforward manner by applying the convolution to a nonlinear transformation of the state.*

Let us now assume that our group action is a shift operation (e.g., $T_g x = x - a \text{ mod } L$). Furthermore, we assume that the partial differential operator \mathcal{N} defined by Eq. (1) does not explicitly depend on space x or time t . We thus obtain shift equivariance of the right-hand side of the PDE

and thus, the group action on the position commutes with the flow Φ^t (Ober-Blöbaum and Peitz 2021, Remark 1):

$$\begin{aligned} y(g^{-1}[x], t) &= g[y](x, t) = \Phi^t(g[y](x, 0)) \\ &= \Phi^t(y(g^{-1}[x], 0)). \end{aligned}$$

Note that the group action g formally transforms the function y which depends on x and t , but acts as the identity on t . Using the convolution observable and the equivariance of the PDE, we find that the corresponding Koopman operator inherits the equivariance property.

Theorem 10. *Consider a PDE of the general form (1) with periodic boundary conditions, where \mathcal{N} does not explicitly depend on space x or time t and is thus equivariant under translations in x (and t) in view of the periodic boundary conditions. Then, the Koopman operator associated with (1) and the observable f_s as defined in (11) is also equivariant under the same group action.*

Proof. Introducing $\tilde{x} = x - a$, we get (under periodic BCs)

$$\begin{aligned} f_{g^{-1}[s]}(y_t) &= z_t(g^{-1}[s]) = \int_{\Omega} y_t(x)\theta(s + a - x) dx \\ &= \int_{\Omega} y_t(\tilde{x} + a)\theta(s - \tilde{x}) d\tilde{x} \\ &= \int_{\Omega} y_t(g^{-1}[\tilde{x}])\theta(s - \tilde{x}) d\tilde{x} \\ &= (g[y_t] \star \theta)(s) = g[(y_t \star \theta)](s) \\ &= g[z_t](s) = g[f_{(\cdot)}(y_t)](s), \end{aligned}$$

where we have exploited the linearity of both the convolution operation and the group action in line four in order to exchange the operations. As a consequence, we also obtain equivariance of the action of the Koopman operator. For any $y_0 \in \mathcal{A}$ with $y_1 = \Phi^\tau \in \mathcal{A}$, we find

$$\begin{aligned} (\mathcal{K}^t f_{g^{-1}[s]})(y_0) &= f_{g^{-1}[s]}(\Phi^t(y_0)) \\ &= g[f_{(\cdot)}(\Phi^t(y_0))](s) \\ &= g[(\mathcal{K}^t f_{(\cdot)})(y_0)](s). \end{aligned}$$

□

What follows is that the same Koopman operator can be applied to different observables f_{s_1} and f_{s_2} , where $s_2 - s_1 = a \in \mathbb{R}$. We can thus compute a Koopman operator for some f_s , and apply the same operator of a shifted version of f_s , which opens up the possibility to pursue *domain decomposition* strategies as they are very common in finite element techniques or numerical solution approaches for PDEs in general. Moreover, we obtain the possibility to decouple the Koopman operator from a specific spatial domain Ω . As long as we remain within domains with periodic boundary conditions, a transfer is possible in a simple and straightforward manner. Moreover, the equivariance can easily be extended to vector-valued convolution observables, cf. Remark 3.

Remark 11. *Related approaches for the exploitation of translational equivariance have been studied for reservoir computing (Pathak et al. 2018) and in the context of reinforcement learning (Peitz et al. 2023; Vignon et al. 2023).*

Practical considerations and numerical examples

In this section, we will compare local Koopman models $\hat{\mathcal{K}}^\tau$ – obtained from q point measurements located in a compact subset of $[0, L]$ (e.g., neighboring grid points in the discretization) – to a global Koopman model $\tilde{\mathcal{K}}^\tau$ which is obtained using the classical full state observable (i.e., we observe the entire numerical grid at once). As briefly mentioned above, these point measurements can be interpreted in terms of Eq. (11) by considering a Dirac delta function as the kernel. This way, we obtain

$$[z_{t,1} = f_{x_1}(y_t) = y_t(x_1) \quad \dots \quad z_{t,N} = y_t(x_N)].$$

We will compare these two models both regarding the Koopman spectrum and the prediction accuracy. In the latter case, Fig. 2 (a) illustrates how the local models \mathcal{K}^τ can be combined to a global model of repeating entries. Conceptually, we simply obtain a number of entirely independent predictors for subsections of \mathcal{Y} . As we always have to deal with approximations of $\hat{\mathcal{K}}^\tau$, it is clear that the approximate solution can quickly lead to inconsistencies with respect to the PDE state, for instance by developing artificial discontinuities. The question is therefore whether we can establish a link between the different local models. A first intuitive approach would be to simply consider overlapping domains. For instance – considering the example of a local model of size three – we can apply the same $\hat{\mathcal{K}}^\tau$ to $\Psi((z_1, z_2, z_3))$ and to $\Psi((z_2, z_3, z_4))$. However, this means that we effectively obtain multiple predictors for the same quantity (in the previous example, z_2 and z_3 are contained in both models). While it is certainly possible to project each of the local systems back onto the coordinates z and then use the average as the predictor, we would still not achieve a coupling between different model instances.

Remark 12. *In fact, if we were able to obtain an exact finite-dimensional approximation of $\hat{\mathcal{K}}^\tau$, then we would quickly run into inconsistencies, as the same matrix would be a predictor for (z_1, z_2, z_3) and for (z_2, z_3, z_4) . A quick calculation then shows that the prediction of any z_i can not depend on any other z_j , which would mean that \mathcal{K}^τ is just a*

$$\begin{aligned} \tilde{\mathcal{K}}^\tau &= \begin{bmatrix} \left[\hat{\mathcal{K}}^\tau \right] \\ \left[\hat{\mathcal{K}}^\tau \right] \\ \left[\hat{\mathcal{K}}^\tau \right] \end{bmatrix} & \tilde{\mathcal{K}}^\tau &= \begin{bmatrix} \left[\hat{\mathcal{K}}^\tau \right] \left[B_r \right] \left[B_l \right] \\ \left[B_l \right] \left[\hat{\mathcal{K}}^\tau \right] \left[B_r \right] \\ \left[B_r \right] \left[B_l \right] \left[\hat{\mathcal{K}}^\tau \right] \end{bmatrix} \\ & \text{(a)} & & \text{(b)} \end{aligned}$$

Figure 2: Schematic of the local Koopman approach. We consider a local Koopman matrix $\hat{\mathcal{K}}^\tau \in \mathbb{R}^{q \times q}$. (a) The same approximation $\hat{\mathcal{K}}^\tau$ can be applied anywhere in the domain such that we obtain a global matrix $\tilde{\mathcal{K}}^\tau$ with identical blocks $\hat{\mathcal{K}}^\tau$. (b) The shaded B terms represent coupling terms to neighboring local models if we pursue a DMDc-like approach.

diagonal matrix. Our interpretation of this dilemma is that inconsistencies cannot be avoided, as in the generic situation, any finite-dimensional approximation is inexact, meaning that the local Koopman models have to be globally inconsistent or yield trivial dynamics.

Instead, a coupling can be achieved in two different ways. The first option is to treat the connection between two neighboring models as it is done in the Dynamic Mode Decomposition with control (DMDc, Proctor, Brunton, and Kutz (2015)), meaning that using a slightly modified regression problem, we obtain a model of the form

$$\Psi((z_{t+\tau,2}, z_{t+\tau,3}, z_{t+\tau,4})^\top) \approx \hat{K}^\tau \Psi((z_{t,2}, z_{t,3}, z_{t,4})^\top) + B_l z_{t,1} + B_r z_{t,5}, \quad (12)$$

where the two terms $B_r, B_l \in \mathbb{R}^{q \times 1}$ are used to treat the left and right neighbors as control inputs to the dynamics.

As the above approach only works for control inputs that enter the original system in a purely linear fashion (Nüske et al. 2023), an alternative approach is to accept that a purely linear approach may be too much to ask for. Instead, a coupling can be achieved by predicting the next state, project from $\Psi(z)$ onto the coordinates z , and then lift again for each system. Due to the project-then-lift step, we “synchronize” the local systems, at the cost of obtaining nonlinear dynamics. Note that if we use kernel EDMD, then this approach is very closely related to Gaussian Process models.

Numerical setup

In the following, we will study the proposed approaches using the Kuramoto-Sivashinsky equation for two different parameter values $\mu > 0$. For the data generation process, we numerically solve (2) using the spectral Galerkin method implemented in the open source package *shenfun* (Mortensen 2018). As a spatial discretization of Ω , we use $N = 32$ Fourier modes, which is equivalent to $N = 32$ equidistant grid points, i.e., we have $\Delta x = \frac{L}{N} = \frac{\pi}{16}$. The time step for the PDE solver is $\Delta t = 0.01$, and we set $\tau = 20\Delta t = 0.2$ for the traveling wave and $\tau = 5\Delta t = 0.05$ for the bimodal fixed-point setting. We collect $M = 1000$ samples from the attractor \mathcal{A} , which yields a sufficient coverage for the considered μ values.

In our experiments, we first compare the PDE solution to the approximation \hat{K} of the global Koopman operator \mathcal{K} , where $f(y) = y$. We then compare this to local Koopman models \hat{K} both in terms of the Koopman spectrum as well as regarding the prediction accuracy. For the latter, we construct a global model \tilde{K} from the local \hat{K} . We do so following both the classical approach (Fig. 2 (a)) and the DMDc approach (Fig. 2 (b)). Following Theorem 4, we study different embedding dimensions, where q_w is the window width (i.e., the number of neighboring points of the discretized PDE), q_d is the number of delays, and the total dimension is $q = q_w \cdot q_d$. The global Koopman model K is thus a special case of \hat{K} where $q_w = N$. We will use standard DMD (i.e., $\Psi = \text{id}$) in all experiments.

Traveling wave ($\mu = 15$)

At $\mu = 15$, the system exhibits a traveling wave solution, as shown in Fig. 3. As this is a very simple behavior, we do not study delay coordinates and set $q_d = 1$, i.e., $q = q_w$. We see in Fig. 3 (bottom) that the DMD approximation (i.e., $\Psi = \text{id}$) is sufficient to yield accurate long-term predictions, even though a slow decay is visible after a while.

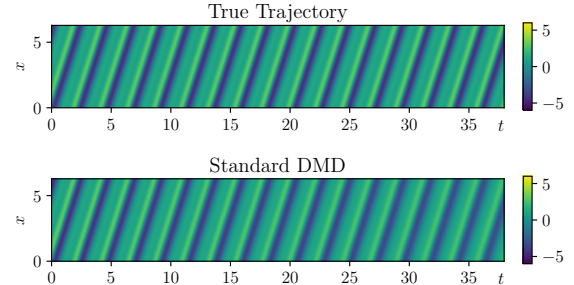


Figure 3: PDE solution vs. global Koopman-approximation for $\mu = 15$. To compute K , we have used the standard DMD algorithm on the full state observable (i.e., $f = \Psi = \text{id}$).

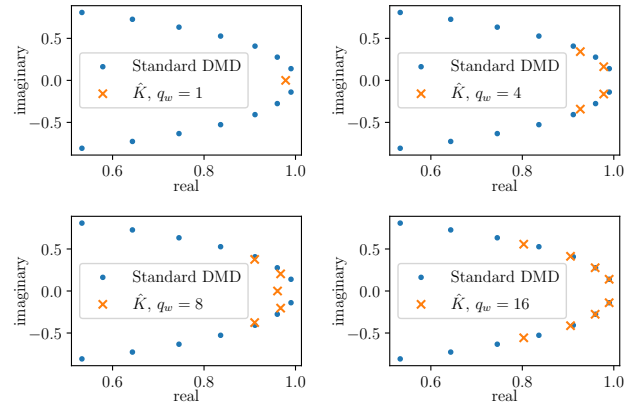


Figure 4: Eigenvalues of K vs. \hat{K} for varying q values.

We next compare K and the local Koopman model \hat{K} for different values of $q_w = q$, varying between $q = 1$ and $q = 16$, which is half of the domain. The corresponding spectra are compared in Fig. 4, and we observe a very good agreement for the leading eigenvalues (the lowest frequency corresponds to the frequency of the traveling wave).

The prediction of the state y using the reconstructed Koopman operator \tilde{K} (according to Fig. 2 (a)) is depicted in Fig. 5. As discussed before, the complete decoupling of the local models \hat{K} yields globally inconsistent dynamics caused by small prediction errors. This is most evident for $q = 4$ and $q = 8$. At $q = 16$, the approximation is sufficiently accurate that we do no longer observe this phenomenon. Interestingly, this decoherence is quite severe even though the one-step prediction error reaches a very small value already at $q = 4$, cf. Fig. 6.

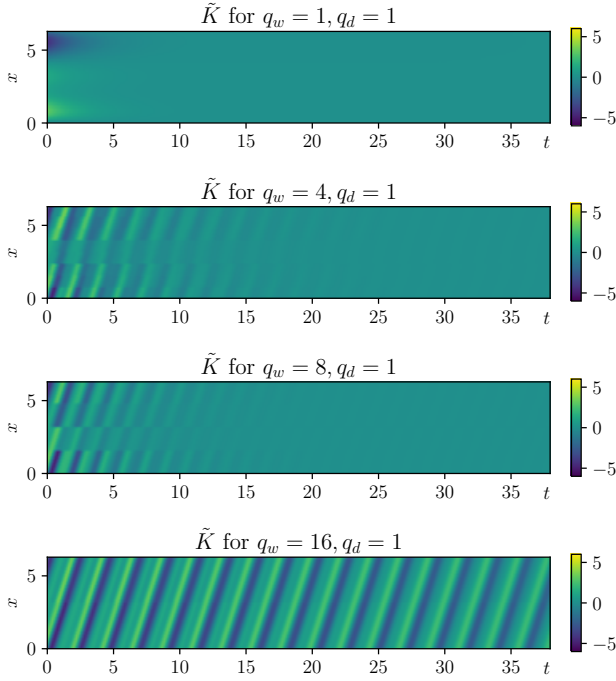


Figure 5: Predictions using \tilde{K} with varying q values.

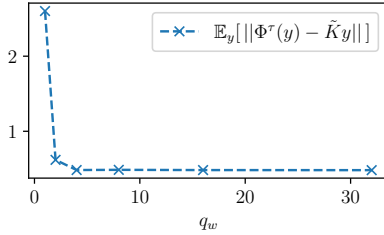


Figure 6: One-step prediction error for varying window widths q_w .

Unsurprisingly, the prediction accuracy improves massively when we build in a coupling term according to Fig. 2 (b) and Eq. (12). Using a single input from left and right, we obtain high-quality predictions using a very small linear system ($q = 1$ and two inputs), see Fig. 7.

Bimodal fixed point ($\mu = 18$)

As a second system, we study the parameter $\mu = 18$ which results in a “checkerboard” pattern. As the dynamics are now much more complex (due to the equivariance w.r.t. translations in space, the attractor consists of infinitely many checkerboard patterns), we here additionally consider $q_d = 50$ delay observations. Using this higher-dimensional observable, many results from the previous case hold in a very similar fashion. Fig. 8 shows a comparison of different approximations, more figures can be found in the appendix.

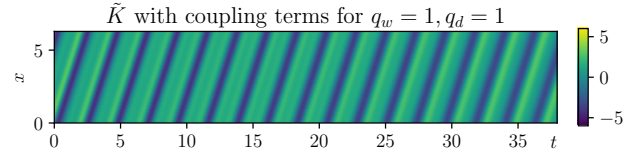


Figure 7: Local DMDc-approximation according to Fig. 2 (b), with $q = 1$ and an additional control input from left and right, respectively.

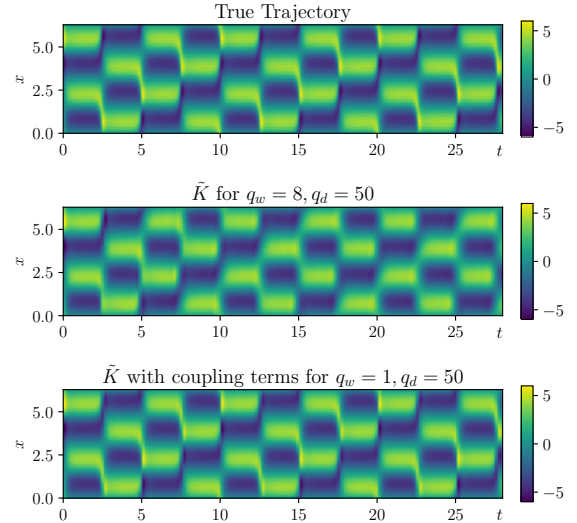


Figure 8: PDE vs. local model with $q_w = 8$ and $q_d = 50$ versus DMDc model with $q_w = 1$ and $q_d = 50$.

Conclusion

We have presented two extensions to the current Koopman theory that deal with (i) the issue of not knowing the system’s state space (i.e., using partial measurements, for instance from sensors) and (ii) the exploitation of symmetries when setting up Koopman-based surrogate models. Regarding part (i), we have shown that there exists a close connection between the Koopman observable function f and observation maps as they are defined in the embedding literature (Takens, Whitney, ...). If we observe sufficiently many points (more than two times the attractor dimension), then we can simply treat our measurements as if they have been generated by another dynamical system with state space \mathbb{R}^q , on which we can then use standard EDMD techniques. This yields rigorous criteria for the situation when building Koopman models exclusively from partial measurements. For part (ii), we have then exploited this in order to simply use q local measurements to build a local Koopman operator approximation. Our numerical results show that including coupling terms (in the spirit of DMD with control) significantly increases the accuracy, even for very small model sizes.

Acknowledgments

S.P. and H.H. acknowledge financial support by the project “SAIL: Sustainable Life-cycle of Intelligent Socio-Technical Systems” (Grant ID NW21-059D), which is funded by the program “Netzwerke 2021” of the Ministry of Culture and Science of the State of Northrhine Westphalia, Germany. K.W. gratefully acknowledges funding by the Deutsche Forschungsgemeinschaft (DFG, German Research Foundation) – Project-ID 507037103.

References

- Avila, A. M.; and Mezić, I. 2020. Data-driven analysis and forecasting of highway traffic dynamics. *Nature Communications*, 11(1).
- Bevanda, P.; Beier, M.; Lederer, A.; Sosnowski, S.; Hüllermeier, E.; and Hirche, S. 2023. Koopman Kernel Regression. *arXiv:2305.16215*.
- Boninsegna, L.; Nüske, F.; and Clementi, C. 2018. Sparse learning of stochastic dynamical equations. *Journal of Chemical Physics*, 148.
- Bronstein, M. M.; Bruna, J.; Cohen, T.; and Veličković, P. 2021. Geometric deep learning: Grids, groups, graphs, geodesics, and gauges. *arXiv:2104.13478*.
- Brunton, S. L.; Budišić, M.; Kaiser, E.; and Kutz, J. N. 2022. Modern Koopman Theory for Dynamical Systems. *SIAM Review*, 64(2): 229–340.
- Brunton, S. L.; Proctor, J. L.; and Kutz, J. N. 2016. Discovering governing equations from data by sparse identification of nonlinear dynamical systems. *Proceedings of the National Academy of Sciences*, 113(15): 3932–3937.
- Budišić, M.; Mohr, R.; and Mezić, I. 2012. Applied Koopmanism. *Chaos*, 22.
- Chorin, A. J.; Hald, O. H.; and Kupferman, R. 2000. Optimal prediction and the Mori–Zwanzig representation of irreversible processes. *Proceedings of the National Academy of Sciences*, 97(7): 2968–2973.
- Dellnitz, M.; Hessel-von Molo, M.; and Zießler, A. 2016. On the computation of attractors for delay differential equations. *Journal of Computational Dynamics*, 3(1): 93–112.
- Hyman, J. M.; Nicolaenko, B.; and Zaleski, S. 1986. Order and complexity in the Kuramoto–Sivashinsky model of weakly turbulent interfaces. *Physica D: Nonlinear Phenomena*, 23(1): 265–292.
- Klus, S.; Koltai, P.; and Schütte, C. 2016. On the numerical approximation of the Perron–Frobenius and Koopman operator. *Journal of Computational Dynamics*, 3(1): 51–79.
- Klus, S.; Nüske, F.; Peitz, S.; Niemann, J.-H.; Clementi, C.; and Schütte, C. 2020. Data-driven approximation of the Koopman generator: Model reduction, system identification, and control. *Physica D: Nonlinear Phenomena*, 406: 132416.
- Koopman, B. O. 1931. Hamiltonian systems and transformation in Hilbert space. *Proceedings of the National Academy of Sciences*, 17(5): 315–318.
- Korda, M.; and Mezić, I. 2018a. Linear predictors for nonlinear dynamical systems: Koopman operator meets model predictive control. *Automatica*, 93: 149–160.
- Korda, M.; and Mezić, I. 2018b. On Convergence of Extended Dynamic Mode Decomposition to the Koopman Operator. *Journal of Nonlinear Science*, 28(2): 687–710.
- Mauroy, A. 2021. Koopman Operator Framework for Spectral Analysis and Identification of Infinite-Dimensional Systems. *Mathematics*, 9(19).
- Mezić, I. 2013. Analysis of Fluid Flows via Spectral Properties of the Koopman Operator. *Annual Review of Fluid Mechanics*, 45: 357–378.
- Mortensen, M. 2018. Shenfun: High performance spectral Galerkin computing platform. *Journal of Open Source Software*, 3(31): 1071.
- Nakao, H.; and Mezić, I. 2020. Spectral analysis of the Koopman operator for partial differential equations. *Chaos: An Interdisciplinary Journal of Nonlinear Science*, 30(11): 113131.
- Niemann, J.-H.; Klus, S.; and Schütte, C. 2021. Data-driven model reduction of agent-based systems using the Koopman generator. *PLOS ONE*, 16(5): e0250970.
- Nüske, F.; Koltai, P.; Boninsegna, L.; and Clementi, C. 2021. Spectral Properties of Effective Dynamics from Conditional Expectations. *Entropy*, 23(2): 134.
- Nüske, F.; Peitz, S.; Philipp, F.; Schaller, M.; and Worthmann, K. 2023. Finite-data error bounds for Koopman-based prediction and control. *Journal of Nonlinear Science*, 33: 14.
- Ober-Blöbaum, S.; and Peitz, S. 2021. Explicit multiobjective model predictive control for nonlinear systems with symmetries. *International Journal of Robust and Nonlinear Control*, 31(2): 380–403.
- Otto, S. E.; Peitz, S.; and Rowley, C. W. 2022. Learning Bilinear Models of Actuated Koopman Generators from Partially-Observed Trajectories. *arXiv:2209.09977*.
- Pathak, J.; Hunt, B.; Girvan, M.; Lu, Z.; and Ott, E. 2018. Model-Free Prediction of Large Spatiotemporally Chaotic Systems from Data: A Reservoir Computing Approach. *Physical Review Letters*, 120(2).
- Peitz, S.; and Klus, S. 2019. Koopman operator-based model reduction for switched-system control of PDEs. *Automatica*, 106: 184–191.
- Peitz, S.; Otto, S. E.; and Rowley, C. W. 2020. Data-Driven Model Predictive Control using Interpolated Koopman Generators. *SIAM Journal on Applied Dynamical Systems*, 19(3): 2162–2193.
- Peitz, S.; Stenner, J.; Chidananda, V.; Wallscheid, O.; Brunton, S. L.; and Taira, K. 2023. Distributed Control of Partial Differential Equations Using Convolutional Reinforcement Learning. *arXiv:2301.10737*.
- Philipp, F.; Schaller, M.; Worthmann, K.; Peitz, S.; and Nüske, F. 2023. Error bounds for kernel-based approximations of the Koopman operator. *arXiv:2301.08637*.
- Proctor, J. L.; Brunton, S. L.; and Kutz, J. N. 2015. Dynamic mode decomposition with control. *SIAM Journal on Applied Dynamical Systems*, 15(1): 142–161.

Raissi, M.; Perdikaris, P.; and Karniadakis, G. E. 2019. Physics-informed neural networks: A deep learning framework for solving forward and inverse problems involving nonlinear partial differential equations. *Journal of Computational Physics*, 378: 686–707.

Robinson, J. C. 2005. A topological delay embedding theorem for infinite-dimensional dynamical systems. *Nonlinearity*, 18(5): 2135–2143.

Rowley, C. W.; Mezić, I.; Bagheri, S.; Schlatter, P.; and Henningson, D. S. 2009. Spectral analysis of nonlinear flows. *Journal of Fluid Mechanics*, 641: 115–127.

Salova, A.; Emenheiser, J.; Rupe, A.; Crutchfield, J. P.; and D’Souza, R. M. 2019. Koopman operator and its approximations for systems with symmetries. *Chaos*, 29: 093128.

Schaller, M.; Worthmann, K.; Philipp, F.; Peitz, S.; and Nüske, F. 2023. Towards reliable data-based optimal and predictive control using extended DMD. *IFAC-PapersOnLine*, 56: 169–174.

Takens, F. 1981. Detecting strange attractors in turbulence. In *Lecture Notes in Mathematics*, 366–381. Springer Berlin Heidelberg.

Vignon, C.; Rabault, J.; Vasanth, J.; Alcántara-Ávila, F.; Mortensen, M.; and Vinuesa, R. 2023. Effective control of two-dimensional Rayleigh–Bénard convection: Invariant multi-agent reinforcement learning is all you need. *Physics of Fluids*, 35(6).

Vlachas, P. R.; Byeon, W.; Wan, Z. Y.; Sapsis, T. P.; and Koumoutsakos, P. 2018. Data-driven forecasting of high-dimensional chaotic systems with long short-Term memory networks. *Proceedings of the Royal Society A: Mathematical, Physical and Engineering Sciences*, 474(2213).

Weissenbacher, M.; Abbott, S.; Garg, A.; and Kawahara, Y. 2022. Koopman Q-learning: Offline Reinforcement Learning via Symmetries of Dynamics. In *39th International Conference on Machine Learning*.

Whitney, H. 1936. Differentiable Manifolds. *The Annals of Mathematics*, 37(3): 645.

Williams, M. O.; Kevrekidis, I. G.; and Rowley, C. W. 2015. A data-driven approximation of the koopman operator: Extending dynamic mode decomposition. *Journal of Nonlinear Science*, 25: 1307–1346.

Zhang, C.; and Zuazua, E. 2023. A quantitative analysis of Koopman operator methods for system identification and predictions. *Comptes Rendus. Mécanique*, 351(S1): 1–31.

Zhang, W.; Hartmann, C.; and Schütte, C. 2016. Effective dynamics along given reaction coordinates, and reaction rate theory. *Faraday Discussions*, 195: 365–394.

Ziessler, A.; Dellnitz, M.; and Gerlach, R. 2019. The Numerical Computation of Unstable Manifolds for Infinite Dimensional Dynamical Systems by Embedding Techniques. *SIAM Journal on Applied Dynamical Systems*, 18(3): 1265–1292.

Appendix

Additional plots for $\mu = 18$

We here show the same figures as for the traveling wave solution at $\mu = 15$. The key difference in the numerical approximation is that we now consider delay observables, i.e., f consists of $q_d = 50$ delays and varying numbers q_w of observed grid nodes.

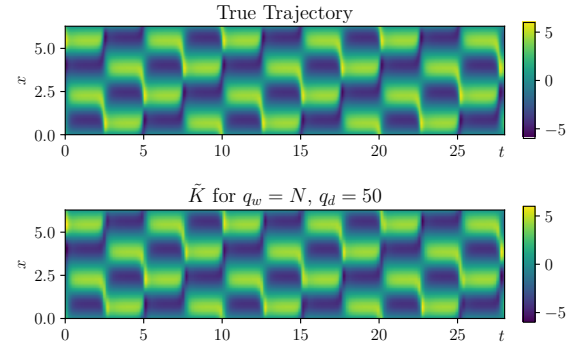


Figure 9: Numerical PDE solution versus global Koopman-approximation for $\mu = 18$.

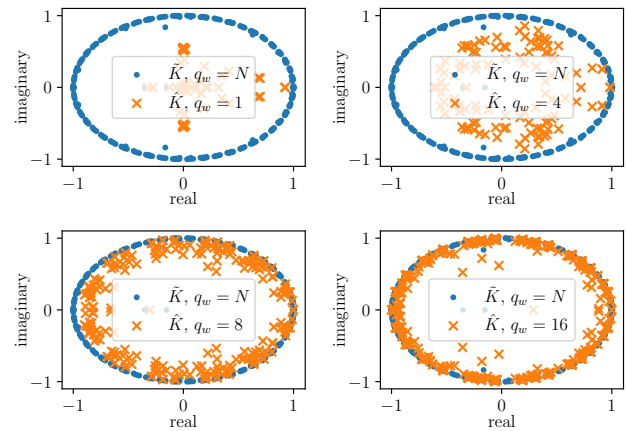


Figure 10: Eigenvalues of K vs. \hat{K} for varying q values.

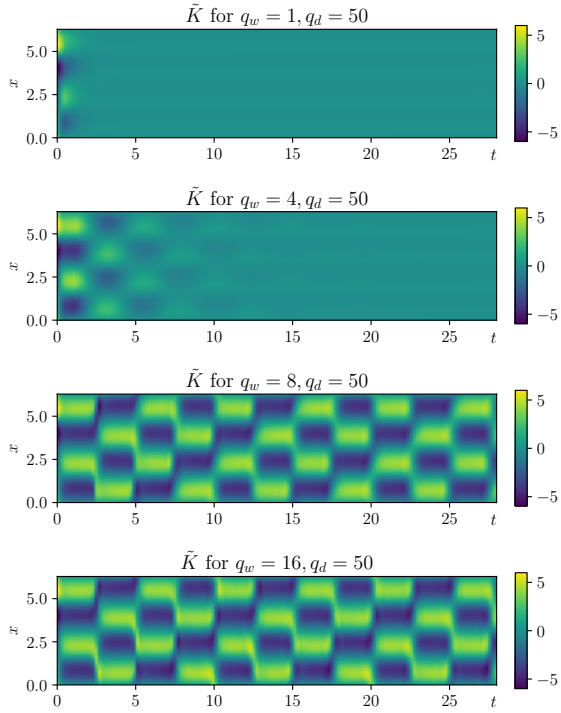


Figure 11: Predictions using \tilde{K} with varying q values.

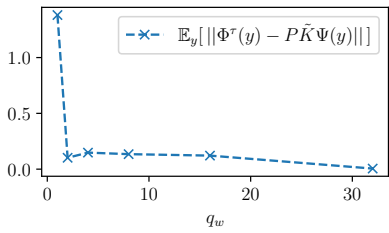


Figure 12: One-step prediction error of \tilde{K} -predictions for varying q values.

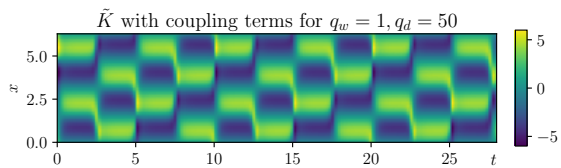


Figure 13: Local DMDc-approximation according to Fig. 2 (b), with $q_d = 50$, $q_w = 1$ and an additional control input from left and right (all $q_d = 50$ delays), respectively.